Published online 10 September 2012 *Nucleic Acids Research, 2012, Vol. 40, No. 21* ***10851–10865***
doi:10.1093/nar/gks833

Common chaperone activity in the G-domain of trGTPase protects L11–L12 interaction on the ribosome

Dandan Zhang[1,2], Guangqiao Liu[1,2], Jiaying Xue[1,2], Jizhong Lou[1], Knud H. Nierhaus[3,4], Weimin Gong[1,2,*] and Yan Qin[1,2,*]

[1]Laboratory of Noncoding RNA, [2]National Laboratory of Biomacromolecules, Institute of Biophysics, Chinese Academy of Sciences, 15 Datun Road, Beijing 100101, China, [3]Max-Planck-Institut für Molekulare Genetik, Abteilung Vingron, AG Ribosomen, Ihnestrasse 73, D-14195 Berlin and [4]Institut für Medizinische Physik und Biophysik, Charité, Universitätsmedizin Berlin, Ziegelstrasse 5-9, D-10117 Berlin, Germany

Received May 8, 2012; Revised August 7, 2012; Accepted August 9, 2012

ABSTRACT

Translational GTPases (trGTPases) regulate all phases of protein synthesis. An early event in the interaction of a trGTPase with the ribosome is the contact of the G-domain with the C-terminal domain (CTD) of ribosomal protein L12 (L12-CTD) and subsequently interacts with the N-terminal domain of L11 (L11-NTD). However, the structural and functional relationships between L12-CTD and L11-NTD remain unclear. Here, we performed mutagenesis, biochemical and structural studies to identify the interactions between L11-NTD and L12-CTD. Mutagenesis of conserved residues in the interaction site revealed their role in the docking of trGTPases. During docking, loop62 of L11-NTD protrudes into a cleft in L12-CTD, leading to an open conformation of this domain and exposure of hydrophobic core. This unfavorable situation for L12-CTD stability is resolved by a chaperone-like activity of the contacting G-domain. Our results suggest that all trGTPases—regardless of their different specific functions—use a common mechanism for stabilizing the L11-NTD•L12-CTD interactions.

INTRODUCTION

The entrance for aminoacyl-tRNAs on the ribosome is surrounded by flexible proteins; one copy of L11 and four to six copies of L7/L12 (1) [L7 is L12 acetylated at its N-terminus (2); L7/L12 is referred to hereafter as L12]. They protrude from the body of the ribosome and extend into the adjacent environment to recruit translational substrates, i.e. aa-tRNA•EF-Tu•GTP ternary complexes, and factors (3–5), and regulate their activities. The C-terminal domain (CTD) of L12 contacts the G-domain of elongation factor G (EF-G), initiating the recruitment of this factor (6–8), and regulates GTPase activation (9–12) and Pi release after GTP hydrolysis (12). The N-terminal domain (NTD) of L11 along with helices 43 and 44 of 23S rRNA (H43/44) forms the target site for thiazole family antibiotics (13–15). The thiazole antibiotics micrococcin (Micro) and thiostrepton (Thio) stimulate and inhibit EF-G-dependent GTP hydrolysis, respectively (16,17). Mechanistic studies reveal that the binding of Thio immobilizes L11-NTD (13–15) and thus prevents the translocation process, which is an EF-G-driven movement of the A and P tRNAs in the pre-translocational (PRE) state to the P and E sites to establish the post-translocational (POST) state. The opposite effect of Micro to Thio is intriguing, since it has a similar structure to Thio and also binds between L11-NTD and H43/44 (13,15,18).

Studies on the dynamics of L12-CTDs have revealed that they undergo boxing-like movements and form identical interactions with the various translational GTPases (trGTPases) (1,4,19,20). Separately, L11-NTD has been found to undergo a swing-like movement upon factor binding and GTP hydrolysis (5). Molecular dynamics (MDs) simulations have revealed additional details: upon EF-G binding, L11-NTD not only swung out as a whole, but its loop region around residue 62 (loop62) extended even further (21). We wondered whether the

*To whom correspondence should be addressed. Tel:/Fax: +86 10 6486 9250; Email: qiny@ibp.ac.cn
Correspondence may also be addressed to Weimin Gong. Tel:/Fax: +86 10 6488 8467; Email: wgong@ibp.ac.cn

The authors wish it to be known that, in their opinion, the first two authors should be regarded as joint First Authors.

movements of L12-CTD and L11-NTD upon factor binding are inherently related.

The interaction between L11-NTD and L12-CTD was deduced from an 11-Å cryo-electron microscope (cryo-EM) map of a POST ribosome containing an EF-G in the presence of fusidic acid (POST•EF-G•FA) (7). Conformation and structural details for this binding interaction were recently provided by X-ray crystallography and cryo-EM of a corresponding functional complex (8,22) and by X-ray crystallography of the 50S ribosomal subunit in complex with Micro (15). In these structures, L11-NTD was connected to L12-CTD by insertion of loop62 into a cleft of L12-CTD. While shedding light on the L11–L12 interaction, the structures did not suggest how this interaction might be established and controlled.

Here, to address this point, we studied molecular details of the L11–L12 interaction and assessed its functional importance. In this process, we found that the hydrophobic core of L12-CTD partially exposed upon its interaction with L11-NTD. This prompted us to analyze whether a chaperone-like activity of the contacting translation factor could stabilize L12-CTD. Our results demonstrate that all trGTPases possess chaperone activity in their G-domains, suggesting a universal mechanism for the L11–L12 interaction, an early event of trGTPase docking onto the ribosome. This mechanism involves both the G-domain of trGTPase and the L11-NTD•L12-CTD interaction in spite of different specific functions of these factors.

MATERIALS AND METHODS

Translational components and the rapid translation system (RTS) were prepared according to (23) and references therein. Reconstitution of L11- or L12-depleted ribosomes with WT or mutated L11 or L12 was performed as described previously (3,12). Citrate synthase (CS), α-glucosidase and other reagents were from Sigma-Aldrich. Micrococcin was prepared as described (24).

Protein expression and purification

Escherichia coli lepA, *fusA*, *rplK* and *rplL* genes, coding for EF4, EF-G, L11 and L12, respectively, were cloned from genomic DNA using PCR primers that introduced NdeI and XhoI restriction sites for cloning into expression vectors. The PCR DNA products coding for EF4, EF4-N2, EF4-N3, EF-G-N2, EF-G-N3, L11 and L12 were cloned into the pET22b vector (Novagen), while the PCR DNA products coding for EF-G, EF-GΔ4, EF4-NTD and EF4-N4 were cloned into the pET28a vector (Novagen). Site mutations of *E. coli* L11, L12, EF-G and EF4 were performed using a TakaRa site-directed mutagenesis kit. All proteins were tagged with His-tags. They were expressed in *E. coli* BL21 (DE3) and induced with 0.1 mM IPTG at 16°C overnight. A nickel column was used in the first round of purification. Concentrated samples were further purified by ion-exchange chromatography and gel filtration using a Sephadex G-75 column. The characteristics of protein in solution were then analyzed by analytical ultracentrifugation and dynamic light scattering. Samples were collected, concentrated and stored at −80°C. *Thermus thermophilus* L11-NTD, L12-CTD and EF4 genes were amplified by PCR using *T. thermophilus* genomic DNA and cloned to the pET-22 b vector using NdeI/NotI restriction sites. *T. thermophilus* L11-NTD, L12-CTD and EF4 proteins were expressed in BL21(DE3), induced with 0.4 mM IPTG at 16°C for 20 h. Cells were disrupted by ultrasound and centrifugation. The soluble cell extract was heat-shock treated by incubation at 65°C for 20 min and the supernatant was further purified by HiTrap-SP and Superdex-75 (GE) chromatography. Protein solutions were concentrated and stored at −80°C. Characteristics of the proteins in solution were analyzed by molecular sieve chromatography, analytical ultracentrifugation and dynamic light scattering. The mutated L11 and L12 proteins were further analyzed by native gel electrophoresis.

Chemical footprinting of *E. coli* 70S ribosome•EF–G•GDPNP complexes

The assay was performed as described previously (24) with some modifications. Prior to tRNA footprinting, 20 pmol of ribosomal complexes were incubated at 37°C for 10 min, then at 0°C for 30 min with the addition of dimethyl sulfate (DMS). Primer extension products of modified rRNAs were separated on 8% polyacrylamide gels.

GTP hydrolysis assays

For ribosome-stimulated uncoupled GTP hydrolysis assays, reconstituted ribosomes (0.2 μM) were mixed with EF-G (0.06 μM) in standard buffer ($H_{20}M_{4.5}N_{150}SH_4Spd_2Sp_{0.05}$) (24) at 37°C for 5 min. The reaction was initiated by the addition of (γ-^{33}P) GTP (75 μM). Solutions containing thiostrepton or micrococcin were prepared (15) and added to reach a final concentration of 5 or 2 μM, respectively.

Green fluorescent protein synthesis assays/coupled transcription-translation assays

RTS 100 *E. coli* HY Kits from Roche were used. For a 50-μl reaction,12 μl of *E. coli* lysate, 10 μl of reaction mix, 12 μl of amino acids, 1 μl of methionine, 5 μl of reconstitution buffer and 1.5 μg of plasmids containing the EGFP gene downstream of the T7 promoter (pIVEX2.3-EGFP) were adjusted to 50 μl with RNase- and DNase-free water. Ribosomes in the *E. coli* lysate were pelleted and replaced by the same amount of reconstituted ribosome with WT or mutated L11/L12. The reaction was run for up to 8 h at 30°C. The amount of synthesized EGFP was determined either by measuring the fluorescence or after separating the proteins on SDS–polyacrylamide gels (SDS–PAGE) and staining with Coomassie Blue. Solutions containing thiostrepton or micrococcin were prepared (15) and added to reach a final concentration of 5 or 2 μM, respectively.

Growth experiments

For individual exponential phase growth experiments, overnight cultures incubated at 37°C in LB medium

were diluted 100-fold and monitored at 600 nm. For competition experiments, L11-depleted cells rescued by WT L11, which were chloramphenicol and kanamycin resistant, were mixed with one of the L11-depleted strains rescued by mutant L11 and the total number of generations was calculated based on the equation below. The estimated percentage of mutant cells was plotted as a function of the number of generations.

$$\frac{\ln A_{260} - \ln 0.01}{\ln 2}.$$

In vitro pull-down assay

N-terminal 6× His-tagged L12 or its mutant proteins (bait protein) (1.6 mM, 20 µl) were immobilized on Ni^{2+} chelate beads in standard buffer and incubated with either *E. coli* cell lysates (40 mg/ml, 20 µl) or purified non-His-tagged L11 mutants (0.4 mM, 20 µl) in the same buffer at 37°C for 30 min. After washing three times with standard buffer and elution with imidazole (100 mM), binding was detected by 15% SDS–PAGE and immunoblotting using anti-L11 (αL11).

Refolding of CS

Denaturation and renaturation of CS were performed as described (25) with modifications. CS (10 µM) was denatured in 6 M GdnHCl, 50 mM Tris–HCl pH 8.0 and 2 mM DTT at 25°C for over 2 h. Renaturation was initiated by a 100-fold dilution in 40 mM HEPES–KOH pH 8.0, 50 mM KCl, 10 mM $(NH_4)_2SO_4$ and 2 mM KAc at 25°C for the times indicated, with or without chaperone and other additives. The activity of renatured CS was determined in 50 mM Tris–HCl pH 8.0, 0.1 mM acetyl coenzyme A, 0.2 mM oxaloacetate and 0.2 mM 5,5′-dithiobis (2-nitro-benzoic acid) (DTNB) by measuring 412 nm absorbance. In all CS assays, the enzyme activity of 0.1 µM native CS after incubation at 25°C for 40 min was set to 100%.

Refolding of α-glucosidase

Denaturation and renaturation of α-glucosidase were performed as described (25) with modifications. α-glucosidase (3 µM) was denatured in 8 M urea, 0.1 M $KHPO_4$ pH 7.0, 1 mM EDTA and 20 mM DTT at 25°C for 1.5 h. Renaturation was initiated by a 30-fold dilution in 40 mM HEPES–KOH pH 7.5, which was then incubated at 25°C for the times indicated, with or without chaperone and other additives. Renatured α-glucosidase (2 µl) was mixed with 57 µl buffer-60 mM $KHPO_4$ pH 7.0, 0.1 mM glutathione (GSH) and 0.9 mM *p*-nitrophenyl α-D-glucoside (PNP-Gluc) and incubated at 37°C for 20 min. A total of 20 µl of the mixture was then added into 80 µl 0.1 M Na_2CO_3 and absorbance at 400 nm was recorded. In all α-glucosidase assays, the enzyme activity of 0.1 µM native α-glucosidase after incubation for 1 h at 25°C was set as 100%.

Thermal aggregation of CS

Thermal aggregation was carried out as described (26) with modifications. Native CS (40 µM) was diluted 200-fold in 40 mM HEPES–KOH pH 7.5 at 43°C in the presence or absence of 0.6 µM factors. CS aggregation was monitored by measuring the absorbance at 320 nm.

Molecular modeling, energy minimization and MD simulations of L12-CTD

Molecular modeling of L12-CTD was performed with VMD (27), while energy minimization and MD simulations of the complex of L11-NTD and the modeled L12-CTD were carried out by using NAMD (28). L12-CTD is poorly solved in the ribosomal crystal structure with the L11-NTD•L12-CTD complex (PDB 2WRL) (22), having a disordered β-sheet region and only a traceable backbone. Thus, to obtain insight into the L11–L12 interaction at the atomic level, we first modeled L12-CTD in the complex conformation based on this poorly solved structure and the structure of the free form of L12-CTD (PDB 1CTF) (29). The modeled L12-CTD structure is denoted as $L12\text{-}CTD^{MD}$. To remove any possible clashes within the modeled structure and with L12-NTD, multiple steps of energy minimization of the L11-NTD•$L12\text{-}CTD^{MD}$ complex were performed and the resulting complex structure was further refined by MDs simulations. The NAMD package (28) and the CHARMM22 all-atom force field (30) were used for energy minimization and MD simulations. A 12-Å cutoff was used for van der Waals interactions and Particle Mesh Ewald summation was used to calculate electrostatic interactions. The energy-minimized system was first equilibrated for 6 ns, with the temperature controlled at 310 K by Langevin dynamics and the pressure controlled at 1 atm with a Langevin piston method followed by 20 ns of free dynamics simulation. During the simulation, the heavy atoms of L11-CTD were constrained. The final snapshot of the MD simulation was used for further analysis.

Multiple alignments

The amino acid sequences were downloaded from PubMed and the alignments were generated by Align-X.

Data analysis

Data in all figures are shown as the mean ± SEM of at least three independent experiments. Statistical significance was evaluated using unpaired two-tailed Student's *t*-test between control/WT and experimental conditions ($^*P < 0.05$, $^{**}P < 0.01$, $^{***}P < 0.001$).

RESULTS

Importance of loop62 of L11-NTD for cell growth and ribosomal functions

According to the crystal structure of the POST state complex with EF-G trapped by FA (*T. thermophilus*) (22), L11-NTD and L12-CTD are located closely together and have the potential to interact with each other. However, due to the lack of side-chain density in L12-CTD, the interactions between L11 and L12 cannot be placed with certainty. Therefore, we first performed molecular modeling of L12-CTD to fit the side chains

from the full-atomic structure of an isolated L12-CTD (*E. coli*; PDB 1CTF) (29) and generated a complete L12-CTD *in situ* (L12-CTD^{MD}) (Figure 1A). The complex of L11-NTD and the modeled L12-CTD was then further refined by MD simulation to remove possible clashes and to search for the most probable positions of the L12-CTD side chains. The resulting structure reveals that L11 contacts L12 by the insertion of its loop62 into the cleft between α-helices 4 and 6 of L12-CTD. The four residues Tyr61, Ala62, Asp63 and Arg64 of loop62 are responsible for this direct interaction. Multiple alignments show that residues 61, 63 and 64 are highly conserved. An aromatic ring (Tyr, Phe and His) side chain is always in position 61, a negatively charged Asp is always in 63 and a positively charged Arg or Lys is always in 64 (Figure 1B). To understand the functional importance of each of the four residues, a series of single mutations was constructed in *E. coli* L11. Of the residue 61 mutants, only the alanine mutant of the L11 protein was achievable; mutation of residue 61 to residues with polar charge or longer hydrophobic side chains made the L11 mutants insoluble. Residue 62 in L11 is generally Ala or a positively charged amino acid, accordingly we constructed an A62K mutant, lysine being the amino acid with the strongest positively charged side chain among the alternatives and obtained an active mutant. Similarly, only short to medium length non-polar side chains at positions 63 and 64 were compatible with an acceptable solubility. We attained a total of four L11 mutants, namely, L11-Y61A, A62K, D63L and R64A, one mutation in each residue of loop62 (Supplementary Figure S1). Each of these L11 mutants was reconstituted into *E. coli* 70S ribosomes lacking L11 protein (70S^{-L11}), and the functions of these ribosomes were assayed.

We investigated whether these L11 mutants had an overall effect on cell growth and viability. To this end we used an *E. coli* strain with a knocked-out L11 gene (*rplK*) carrying a plasmid with either a wild-type (WT) or mutant-L11 gene. Figure 1C shows that all mutants were viable and that the generation time of the L11-D63L mutant was 0.5-fold longer than that of the WT; the corresponding values were 0.33 for L11-Y61A and R64A, and 0.25 for L11-A62K. The superiority of cells harboring WT L11 over those containing mutant L11 was analyzed in growth competition experiments, where equal amounts of WT cells and mutant cells (corresponding to 100% in Figure 1D) were mixed and the relative amounts of both cell types were monitored over several generations. Figure 1D shows that the proportion of L11-D63L cells was dramatically reduced to 1% after 5 generations, while that of the L11-Y61A, R64A and A62K cells was down to 0.1, 0.2 and 0.4% after 12 generations. It is clear that loop62 mutants strongly impair cell performance; mutant cells would be outcompeted by WT cells within several hours in nature.

The effects of loop62 mutations on overall protein synthesis *in vitro* were analyzed in a coupled transcription/translation system (RTS) programmed for green fluorescent protein (GFP) synthesis (Figurer 1E). Again, mutation L11-D63L of the most conserved residue (63) caused the highest reduction (~60%), while L11-A62K showed the lowest reduction (~40%). When Thio or Micro was added to the reaction mix, the 70S^{-L11} + WT-L11 ribosomes were reduced by 60 and 80%, respectively. Thio, by fixing L11-NTD to H43/44, prevents the movement of L11-NTD and its potential interaction with L12-CTD (13,14). Micro, on the other hand, bound to the same region but with a slightly different binding orientation. It thus facilitates an abnormal interaction between L11-NTD and L12-CTD (15) which inhibits protein synthesis, specifically the translocation reaction. In this assay, loop62 mutations exhibited an inhibitory effect comparable to that of Thio.

Do the loop62 mutants affect the binding characteristics of EF-G with the ribosome? This question was assessed by chemical footprinting. L11-NTD has been shown to locate closely to the G-domain and domain V of EF-G (22). Accordingly, we tested the protection patterns of EF-G on the A2660 or A1067 nucleotides of 23S rRNA. These bases are the checkpoints for the G- and V domains, respectively, of bound EF-G (31). Compared to the WT 70S or 70S^{-L11} reconstituted with WT-L11 (70S^{-L11} + L11), the 70S^{-L11} reconstituted with mutants L11 (70S^{-L11} + L11-mutant) provided the same protection of both A2660 and A1067 upon EF-G binding (Figure 1F). These results suggest that L11 mutants do not affect the overall location of EF-G on the ribosome.

We then assayed the ability of L11-mutated ribosomes to stimulate EF-G-dependent GTP hydrolysis. 70S^{-L11} + L11 ribosomes, alone or in the presence of Thio or Micro, were used as controls. Figure 1G shows that loop62 mutants impair GTPase by ~10% (L11-A62K), ~25% (L11-Y61A and R64A) and ~40% (L11-D63L). Thio inhibited 65% of the activity and Micro stimulated activity by 30%. The results suggest that loop62 mutations impair the interaction between L11 and L12 in a similar manner as Thio. Of the four residues, mutation of the most conserved residue Asp63 produced the most serious deficiency. In contrast, lysine mutation of the least conserved 62 Ala residue caused only mild inhibition.

We then carried out *in vitro* pull-down assays and structural analyses to gain more insights into the interactions between L11-NTD and L12-CTD.

An open conformation of L12-CTD exposing hydrophobic core is required for L11–L12 interaction

Direct interaction between L11 and L12 was detected by *in vitro* pull-down coupled to immunoblotting against L11 antibody. N-terminal 6× His-tagged L12 protein (bait) was immobilized on Ni^{2+} chelate beads and incubated with either *E. coli* cell lysate or purified non-His-tagged L11 mutants. The presence of L11 was detected with anti-L11 (αL11). Figure 2A shows the interaction between L11 and L12. Non-specific interaction can be excluded since the empty beads incubated with non-tagged L11 did not show any signal. In Figure 2B, the immobilized L12 was incubated with WT-L11 or the L11 mutants. The L11-D63L mutation did not bind to L12, and L11-Y61A and R64A showed much weaker binding, while L11-A62K bound like WT-L11. The binding pattern nicely reflects the corresponding effects

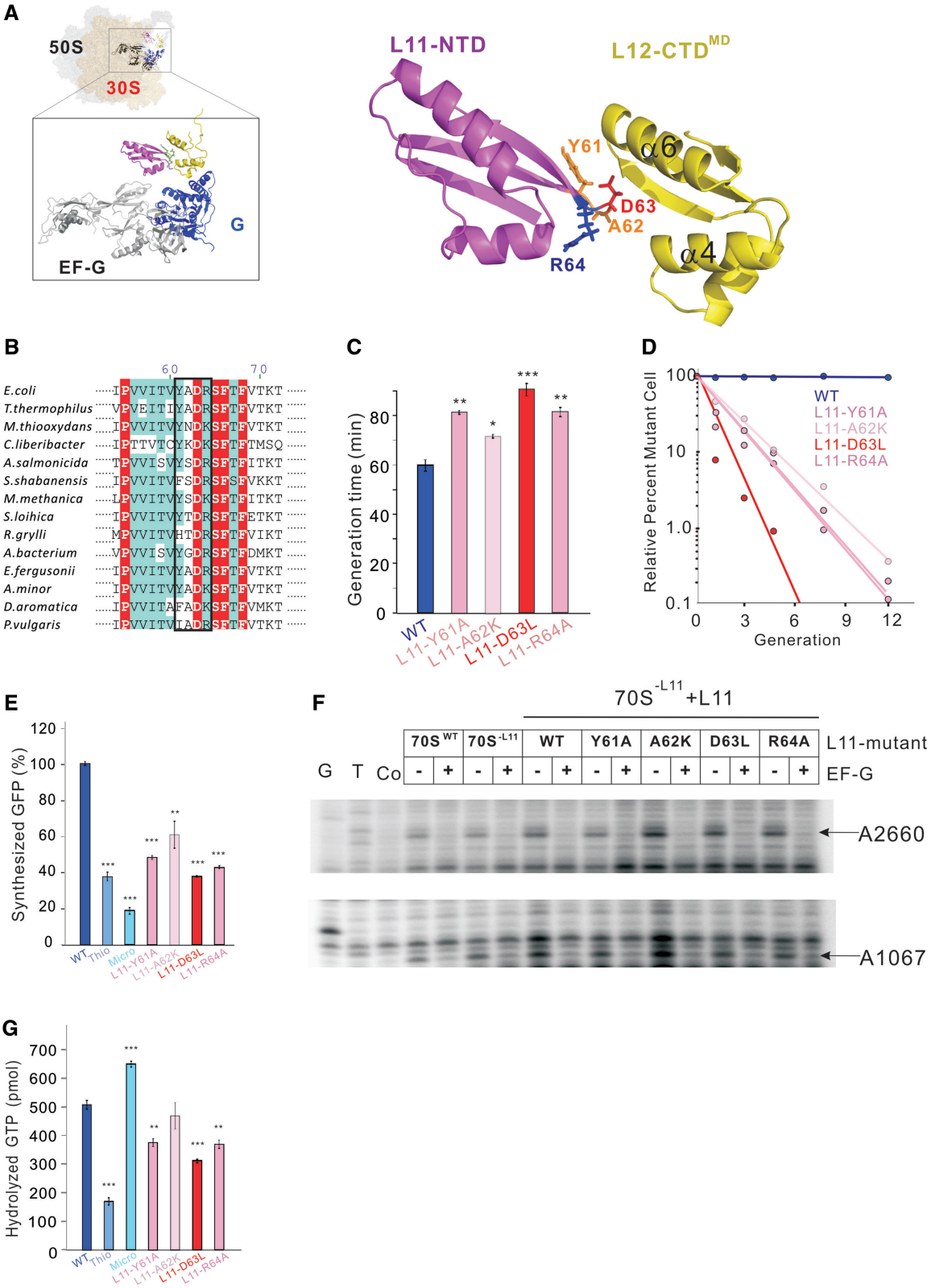

Figure 1. Functional significance of loop62 in translation. (**A**) The crystal structure of 70S•EF-G•FA in POST state (PDB 2WRL) (22) shows that EF-G is located between L12-CTD and L11-NTD. MD simulations reveal details of the L11-NTD•L12-CTD interaction. Loop62 of L11-NTD (magenta) inserts into the cleft between α-helixes 4 and 6 of L12-CTD (yellow). Four residues on loop62, Tyr61 (Y61), Ala62 (A62), Asp63 (D63) and Arg64 (R64), interact directly with L12-CTD^{MD}. (**B**) Multiple alignments show that residues 61, 63 and 64 are highly conserved. Red residues show 100% identity, while blue residues show 80% identity. (**C** and **D**) *In vivo* analyses of loop62 mutations on cell growth. (**C**) The doubling time of *rplK* knock-out *E. coli* cells which are rescued by WT L11 or its mutant (L11-Y61A, A62K, D63L or R64A). (**D**) Equal amount of the *rplK* knock-out *E. coli* cells rescued by WT L11 or its mutant were grown as indicated and the proportion of mutant cells (%) was determined.

(continued)

on growth, protein synthesis and EF-G-dependent GTPase activity shown in Figure 1.

To study the dynamics of the interface between L11-NTD and L12-CTD in solution, we performed nuclear magnetic resonance (NMR) spectroscopy. Each amino acid residue of ^{15}N-labeled L11-NTD (*T. thermophilus*) was assigned according to (32) (Supplementary Figure S2A). We then titrated L12-CTD (*T. thermophilus*) into the L11-NTD solution and generated a ^{1}H-^{15}N heteronuclear single-quantum coherence (HSQC) spectrum at each titration point (Supplementary Figure S2B–S2F). Unexpectedly, no distinct difference was uncovered upon L12-CTD addition, neither chemical shifts nor intensity changes of individual cross-peaks. These results suggested that L11-NTD (*T. thermophilus*) did not contact L12-CTD (*T. thermophilus*) under these conditions. This phenomenon contradicts the reported POST•EF-G•FA (*T. thermophilus*) structure and our L12 pull-down study with *E. coli* proteins shown in Figure 2A and B. To explore the reasons, we compared the structures of isolated L11-NTD and L12-CTD domains with those of their counterparts in the POST•EF–G•FA complex.

The interaction of L11-NTD with L12-CTD on the ribosome triggers two conformational changes: (i) an extension of loop62 of L11-NTD as we reported recently (34) and (ii) a large conformational change in L12-CTD as we found here. When L12-CTD on the ribosome complex (PDB 2WRL) was replaced by its isolated structure (PDB 1CTF) (29), the domains clashed at the connection site (Figure 2C). When we aligned L12-CTD^{MD} (Figure 1A) with its free structure at helix 6 (α6), a distinct open conformation was observed. The tip of helix 4, i.e. the C_α of Gly74, moved 6.4 Å. The angle opened 32.4° between helices 4 and 6, as measured by the angle between the lines connecting Ala113:C_α and Gly74:C_α in the two states (Figure 2D). Surface display reveals that the open conformation of L12-CTD on the ribosome is accompanied by the exposure of the hydrophobic core (compare the closed and open conformations of the L12-CTD in Figure 2E and F, respectively). A detailed map (Figure 2G) demonstrates that residues Asp63 of L11-NTD and Lys95 of L12-CTD are located at the interface. Adjacent to it we see that the exposed hydrophobic core of L12-CTD consists of the residues Leu58, Leu94, Leu106 and Leu110, which are highly conserved (Supplementary Figure S3). Such a conformation is not stable and threatens the integrity of L12-CTD causing it to unfold. This observation provides an explanation of why we could not find an interaction between L11-NTD and L12-CTD in the NMR titration assay. For *T. thermophilus* L12-CTD, an assay temperature of 298 K could be too low to allow a dynamic equilibrium between the unfavorable open state and the stable closed state. The situation did not change, when we increased the temperature to 318 K. When we switched to the *E. coli* counterpart, the low resolution did not allow an assignment. To clarify the molecular details, we resorted to mutagenesis and biochemical methods.

Both electrostatic and hydrophobic forces contribute to the L11–L12 interaction

To identify the main factor responsible for the L11–L12 interaction, we constructed additional mutants of loop62 from L11-NTD. Since the above-mentioned L11-A62K mutation produced unexplainable results for L11-Asp63•L12-Lys95, a potential electrostatic pair, we mutated a neighboring residue of Asp63, i.e. Arg64 to Lys and obtained a soluble L11-R64K mutant (Supplementary Figure S1). Different from its L11-R64A mutation, the L11-R64K mutation strengthened the interaction between the two proteins (Figure 3A). The band intensity (pixel counting) increased ~1.5-fold compared to WT + WT (L11^{WT} with L12^{WT}). In water, the pKa of Arg and Lys are 12.5 and 10.5, respectively. Exchanging Arg to the weaker base Lys enhanced the interaction, suggesting that L11-Arg64 might provide a repulsive force against L12-Lys95. When this residue was exchanged to a weaker base, the repulsive force decreased and thus the interaction between L11-Asp63 and L12-Lys95 was strengthened. This observation partially supports the electrostatic hypothesis and explains the evolutionary conservation of the nature of the side chain of residues 63 (Asp) and 64 (Arg or Lys) of loop62 in L11-NTD and residue 95 (Lys) in L12-CTD. The contribution of Lys95 (L12-CTD) was then ascertained using the L12-K95A mutant, which was soluble (Supplementary Figure S4) and prevented domain interaction (Figure 3A) as observed before with the L11-D63L mutant (Figure 2B).

The influence of L12-CTD's hydrophobic core residues on the L11–L12 interaction was analyzed further. The structure of L12-CTD^{MD} (Figure 2G) reveals that Leu94 stacks with Leu106 and L110, thus drawing β-sheet 2 (β2) close to α6. Similarly, hydrophobic stacking also exists between Leu58/Leu94 and Leu110, thus drawing β1 close to β2 and α6. When we constructed an alanine mutation for each Leu, only L12-L106A could be kept in solution (Supplementary Figure S4). Changing the side chain of one of the other three Leu residues to Ala had strong effects on L12-CTD folding, reflecting the importance of each Leu for the hydrophobic core formation. When the soluble L12-L106A mutant was incubated with WT L11, no interaction was detected (Figure 3A)

Figure 1. Continued

(**E–G**) Importance of loop62 for protein synthesis. WT L11 (deep blue), L11-Y61A (pink), L11-A62K (light pink), L11-D63L (red) or L11-R64A (pink) L11 mutants were reconstituted into ribosomes lacking L11. Ribosomes reconstituted with WT L11 were incubated with Thio (blue) or micrococcin (ice blue). (**E**) Quantification of the total effect of each mutant on GFP synthesis in the RTS system. (**F**) Chemical footprinting of *E. coli* 70S ribosome•EF-G•GDPNP complexes. G and T, sequencing lanes; Co, control without DMS modification; 70S^{WT}, WT ribosome; 70S^{-L11}, the ribosome depleted of L11; 70S^{-L11} + L11, the ribosome depleted of L11 was reconstituted with WT L11 or the L11 mutant as indicated. The EF-G protection pattern of A2660 and A1607 of 23S rRNA is indicated by arrows. (**G**) GTP hydrolysis by EF-G is given as the amount of GTP hydrolyzed in 5 min per ribosome. Error bars represent the mean ± SEM of data from at least three separate experiments. *P*-values were calculated with unpaired *t*-tests using Welch's correction by comparing to WT samples (*$P < 0.05$, **$P < 0.01$, ***$P < 0.001$). See also Supplementary Figure S1.

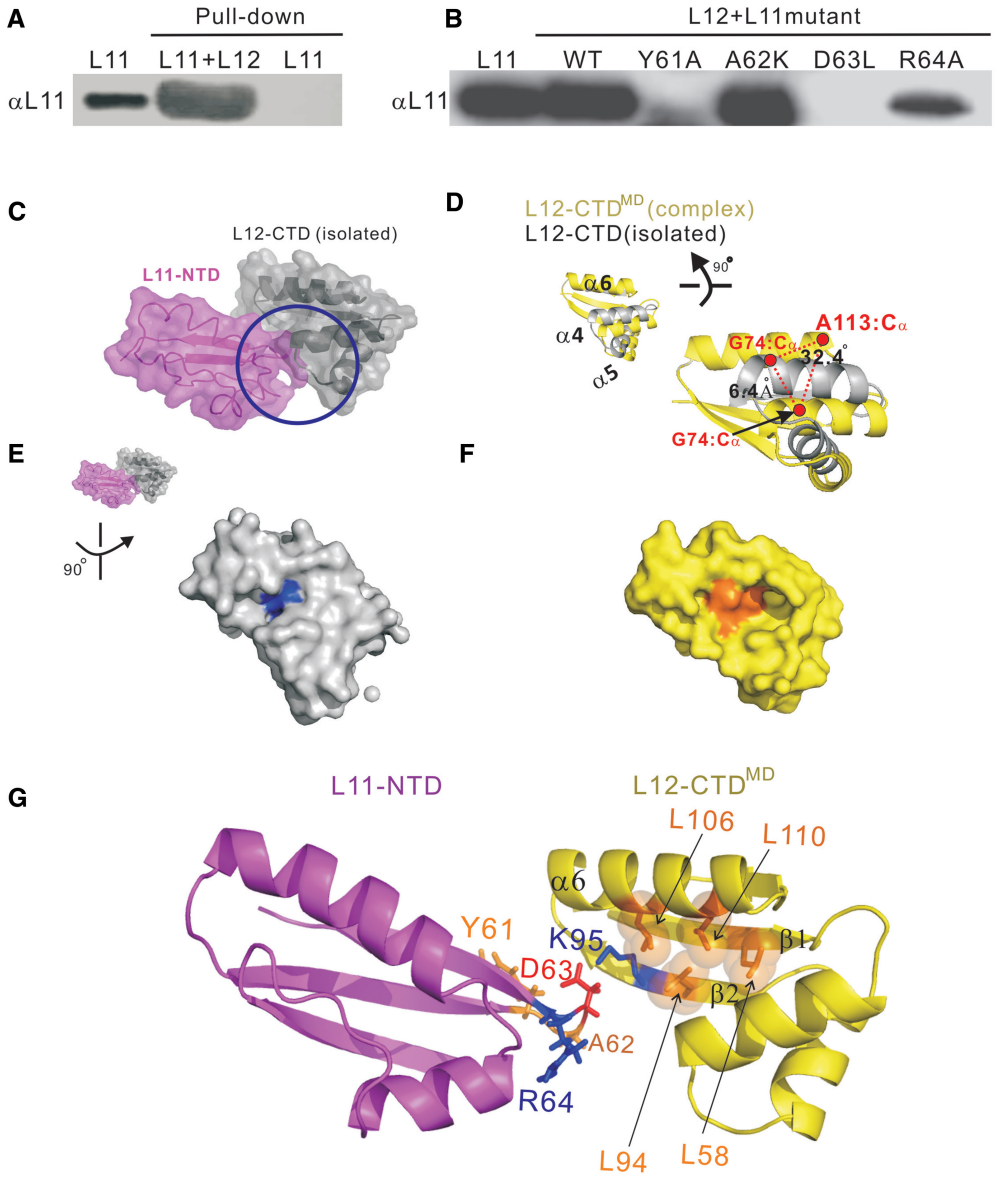

Figure 2. Direct interaction between L11 and L12 requires L12-CTD to be in an open conformation with the hydrophobic core exposed. (**A** and **B**) Interactions between 6× His-tagged L12 and L11 WT (A) or mutants (B) were detected by *in vitro* pull-down assay coupled to immunoblotting against the L11 antibody (αL11). Purified L11 protein was loaded in the first lane (L11) as a marker. (A) Pull-down assays show that L11 binds with L12. No L11 was detected in the control (the third lane) when L11 was incubated with empty beads. (B) The bait-prey pair was the L12+L11 mutant. The D63L mutant did not bind with L12 at all. Y61A and R64A mutants bound a lower intensity, whereas the A62K mutant bound with intensity similar to WT L11. (C–F) Structural comparison of L12-CTD in the isolated state (gray) and on the ribosome (yellow). (**C**) When L12-CTD on the ribosome complex (PDB 2WRL) (22) was replaced by its isolated structure (PDB 1CTF) (29), the interplay between L11-NTD (magenta) and L12-CTD was hindered by a steric clash at the connection site (circled region). (**D**) Structural alignment shows L12-CTD on the ribosome with a more open conformation. When the two structures were aligned to helix 6 (α6), the tip of helix 4, i.e. the C_α of G74, moved 6.4 Å and the helices opened 32.4° more, as measured by the angle of A113:C_α to G74:C_α in the two states. (**E**, **F**) Surface display of L12-CTD with its hydrophobic core in blue (E) or orange (F) in the closed and open states, respectively. (**G**) The interface between L11-NTD and L12-CTD in the open state. The interface is composed of Y61 (orange), A62 (orange), D63 (red, negative charged) and R64 (blue, positive charged) from L11 and K95 (blue, positive charged) from L12. The hydrophobic core of L2-CTD includes L58, L94, L106 and L110 (orange). See also Supplementary Figures S2 and S3.

suggesting that although this mutation did not influence the overall structure of L12-CTD, it strongly weakened the affinity of the domain to L11-NTD.

The reason and consequences of such an affinity drop were then analyzed *in situ* by reconstituting the mutant protein into the ribosome. Tested in parallel with the L11-R64K mutant and the L12-K95A mutant, which strengthened and disrupted the L11–L12 interaction, respectively, L12-L106A had a similar effect on the factor binding of the mutated ribosome, GTP hydrolysis by EF-G and GFP synthesis (Figure 3B–D). The results of this set of mutations were comparable with the loop62 mutants in Figure 1: the new mutants inhibited EF-G-dependent GTPase activity and thus hindered

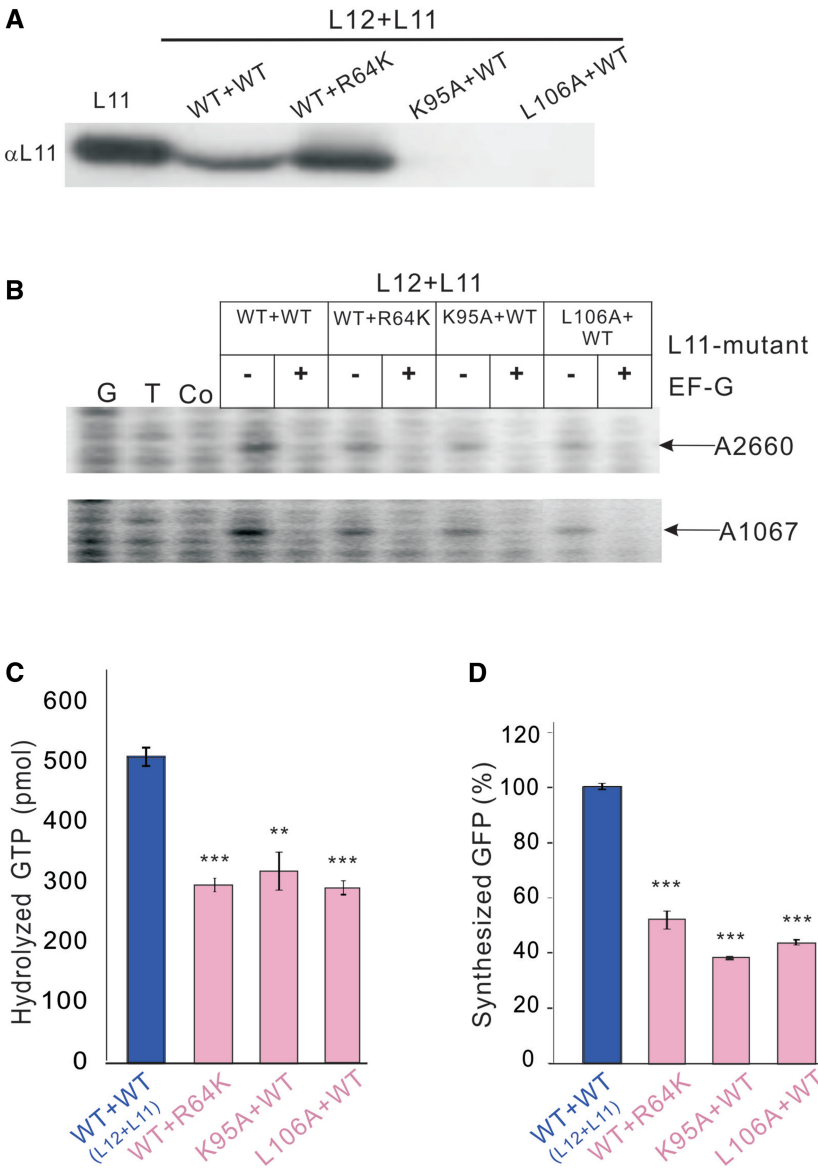

Figure 3. Both electrostatic and hydrophobic forces contribute to the L11–L12 connection. (**A**) An interaction between L11 (WT or mutant) and L12 (WT or mutant) was detected by pull-down assays as described in Figure 2A and B. The bait–prey pair is indicated as L12 + L11 (L12 = WT or K95A or L106A; L11 = WT or R64K). When Arg64 of loop62 was mutated to Lys, the interaction between L11 and L12 was enhanced. When Lys95 of L12 was replaced by Ala, the interaction vanished. Similarly, the L106A mutation abolished the interaction as well. (**B**) Chemical footprinting of *E. coli* 70S ribosome•EF-G•GDPNP complexes. G and T, sequencing lanes; Co, without DMS modification. 70S reconstituted with L11 or L12 are indicated as in (**A**). The EF-G protection pattern of A2660 and A1607 of 23S rRNA is indicated by arrows. (**C** and **D**) Importance of the L11–L12 interaction for EF-G-dependent GTP hydrolysis and protein synthesis, respectively. WT L12 and WT L11 are shown in deep blue and all other combinations in pink. The corresponding proteins L12 and L11 were reconstituted into ribosomes lacking L11 and L12. (**C**) GTP hydrolysis by EF-G is given as the amount of GTP hydrolyzed in 5 min per ribosome. (**D**) The total effect of each mutant on GFP synthesis was quantified in the RTS system. Error bars represent the mean ± SEM of data from at least three separate experiments. *P*-values were calculated with unpaired *t*-test using Welch's correction by comparing to WT + WT samples (**$P < 0.01$, ***$P < 0.001$). See also Supplementary Figure S4.

total protein synthesis. These observations suggest that the hydrophobic contribution of the conserved Leu residues of L12-CTD plays an important role not only in the domain conformation but also in the interplay with L11-NTD.

The L11-R64K mutant was an exception. While it strengthened the L11–L12 interaction, its *in situ* influence on the ribosomal function was the same as the other L11 mutants (Y61A, D63L or R64A) or L12 mutants (K95A or L106A) which weakened the L11–L12 interaction. Medium affinity is obviously more favorable for the establishment of a dynamic connection–disconnection equilibrium, both of these two states being needed for factor regulation on the ribosome. Our series of mutations in the contact regions of both L11-NTD and L12-CTD reveal that both electrostatic and hydrophobic forces play a role in the interaction. Moreover, the non-polar side-chain stacking was found to stabilize the L12-CTD

structure. Upon interaction with L11-NTD, L12-CTD opened and exposed the central hydrophobic region. Such a situation threatens the integrity of the loosely folded and highly dynamic L12-CTD structures and causes unfolding. It is well documented that, in similar situations, chaperones that facilitate protein folding, protect protein conformation and trigger partial unfolding to make proteins transport competent (35), come into play. On the other hand, translation factors EF-Tu and EF-G (25,36) have been reported to possess chaperone activity, although their catalytic centers and target molecules remain elusive. Our data may provide a clue to clarify the inherent relationship between the L11–L12 interaction and the chaperone properties of EF-Tu and EF-G. If the demonstrated chaperone activity of both these EFs is indeed related to the transient exposure of the hydrophobic core of L12-CTD shown here and thus might represent a general feature of the early interaction of EF-Tu and EF-G with the ribosome, then we would expect that all trGTPases should possess such a chaperone activity. This hypothesis is investigated in the following sections.

Identification of EF4 chaperone activity

We reported earlier that EF4 (LepA) is a highly conserved translation factor, catalyzing the POST state ribosomes to PRE state in the reverse direction to EF-G triggered translocation (23). The sequence and structural similarity of EF4 and EF-G (37) promoted us to compare the potential chaperone activity of EF4 and EF-G. In the CS refolding assay, EF4 and EF-G showed an equal ability to facilitate refolding of denatured CS (Figure 4A). Since both factors are classical G-proteins that are able to adopt a GTP conformation (ON state) and a GDP conformation (OFF state), we analyzed the influence of guanosine nucleotides on the potential chaperone activity of EF4. As shown in Figure 4B, neither of them had any impact. Due to the instability of GTP in solution, we repeated the experiments with a non-hydrolysable GTP analogue, GDPNP, and found the same results as with GTP: the chaperone activity of EF4 is independent of guanosine nucleotides and the presence of 70S ribosomes (Figure 4C). Corresponding results were observed in α-glucosidase refolding assays (Figure 4D). The influence of EF4 against thermal aggregation of CS at 43°C was tested and monitored by the light scattering at 320 nm. Without EF4, CS aggregation continued for over 3000 s. When either EF-G or EF4 was added, CS aggregation was reduced. In the reaction after 2000 s, EF4 was able to completely repress thermal aggregation (Figure 4E). These results demonstrate the chaperone activity of EF4.

Common chaperone activity on the G-domains of all trGTPases

Given that the L11–L12 interaction plays an important role in protein biosynthesis, we expect that catalysis of this interaction may be a general feature of translation factors. We therefore analyzed the chaperone activity of all the universal translation factors. Our analysis revealed two groups: one group included IF2, EF-Tu, EF-G, EF4 and RF3 and had chaperone activity, while the other group, which includes the rest of the translation factors, displayed activity values close to that of the negative control in both the CS and α-glucosidase refolding assays (Figure 5A and B). Neither guanosine nucleotides nor the ribosome had any impact on the chaperone activities of these factors (Supplementary Figure S5). It is notable that trGTPases are the only factors that possess chaperone activity.

Based on the characteristics of the G-domain, trGTPases fall into two subclasses: one is represented by EF-G and the other by EF4. EF-G and RF3 possess a G-domain with an extension (G′-domain) in contrast to the typical G-domain of EF4 and the other trGTPases. To locate the catalytic center in the two subclasses of trGTPases, we performed systematic truncations of EF-G and EF4 by deleting domain(s) one by one from the CTD to the NTD (Figure 5C and D). Except for the G-domain of EF-G that precipitated, all truncated mutants were soluble. In the CS refolding analyses, all truncation mutants exhibited chaperone activity (Figure 5E and F) and was confirmed in the α-glucosidase refolding experiments (Figure 5G and H). It is interesting to note that there was always chaperone activity when the NTD was present, suggesting that the chaperone activity of trGTPases is located in the G-domain.

Finally, the residues contributive to the chaperone activity of trGTPases were analyzed by mutagenesis. First, the potential residues were selected by structural information and MD calculation. Then, each residue was point mutated and the resulting mutant was assayed in the protein refolding systems. The results indicated that single mutations did not affect the chaperone activity very much (Supplementary Table S1, single-point row). Next, we constructed more mutants by multiple-point mutation or region deletion. The former mutants exhibited slight chaperone activity decease and the latter ones had the tendency to precipitate in the reaction systems (Supplementary Table S1, multiple-point and deletion rows). Chaperone molecules generally function by providing a hydrophobic region to protect the exposed hydrophobic surface and to facilitate protein refolding. Such function may be not contributed by specific one or two residues, but an area composed of several secondary structures or even more comprehensive components. When one or several conserved residues in this region had been mutated, it did not impair the chaperone activity much. But with region deletion, the conformation of the domain or even the protein might have been disrupted, thus we could not succeed in getting soluble proteins. So, our conclusion stands that G-domain is responsible for the chaperone activity of trGTPases, but the specific amino acid residues contributive to the catalytic activity were not detectable.

TrGTPase facilitates L11–L12 interaction *in vitro*

The 3D structures tell us that the G-domain of EF-G is in contact with L12-CTD, thus initiating the recruitment of EF-G onto the ribosome. It has been demonstrated that trGTPases IF2, EF-Tu, EF-G and RF3 have similar

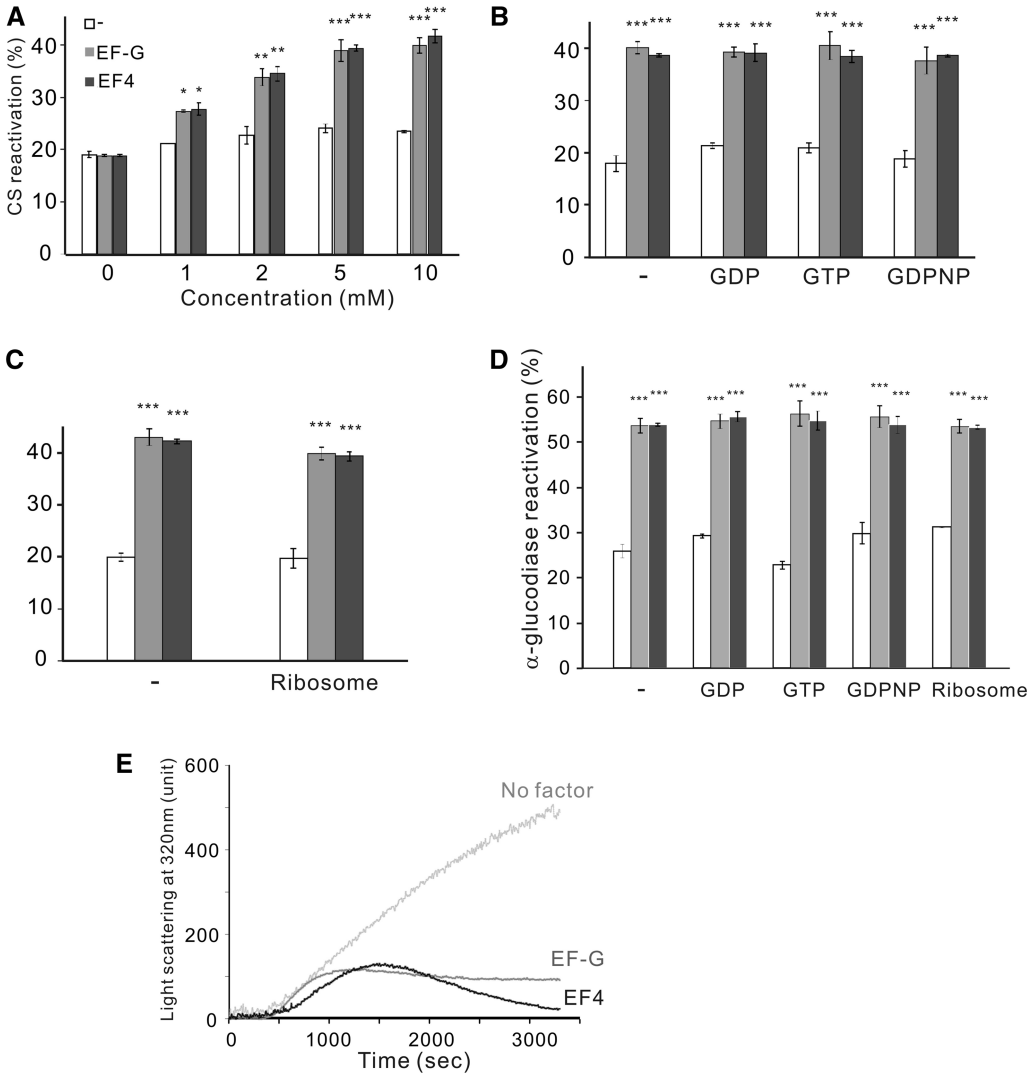

Figure 4. Identification of EF4's chaperone activity. Denatured protein in the absence (empty column) and presence of EF-G (gray) or EF4 (black) was studied in the refolding assay. (**A**) 0.1 μM denatured CS was incubated in the absence and presence of EF-G or EF4 at the indicated concentrations. (**B**) Influence of guanosine phosphates on the chaperone activity of EF4. A total of 0.1 μM denatured CS and 5 μM EF-G or EF4 were incubated in the absence (−) and presence of 2 mM GDP, GTP or its non-hydrolysable analogue GDPNP. (**C**) Influence of the ribosome on the chaperone activity of EF4. A total of 0.1 μM denatured CS and 5 μM EF-G or EF4 were incubated in the absence (−) and presence of 0.2 μM 70S ribosomes. (**D**) Influence of EF4 on the refolding of denatured α-glucosidase. Denatured α-glucosidase (0.1 μM) in the absence and presence of 5 μM EF-G or EF4, with 2 mM GDP, GTP or GDPNP, or with 0.2 μM 70S ribosomes. (**E**) Influence of EF4 on the thermal aggregation of CS. The aggregation of CS at 43°C was monitored by light scattering at 320 nm. Light gray: no chaperone added; gray: EF-G; black: EF4. Error bars represent the mean ± SEM of data from at least three separate experiments. *P*-values were, calculated with unpaired *t*-test with Welch's correction by comparing to EF-G or EF4 samples (*$P < 0.05$, ** $P < 0.01$, ***$P < 0.001$).

interaction patterns with L12-CTD in solution (20). We wondered whether the recently discovered EF4, which is one of the most conserved trGTPases (23), also interacts with L12-CTD. So, we performed a detailed study of the dynamic interplay between L12-CTD and EF4 in solution using NMR. Each amino acid residue of ^{15}N-labeled L12-CTD (*E. coli*) was assigned (Supplementary Figure S6). *E. coli* EF4 was then titrated into L12-CTD, however since EF4 proteins precipitated under the applied condition, we exchanged to *T. thermophilus* EF4, whose solubility and stability is better and obtained a ^{1}H–^{15}N HSQC spectrum at each titration point (Figure 6A). During EF4 titration, a subset of cross-peaks showed gradual changes in chemical shifts. The corresponding residues are in two regions of L12-CTD, 66–70 and 80–85. Representative residues with significant chemical shift changes are shown in Figure 6B. Binding affinities between L12-CTD and EF4 were estimated based on these data and the resulting dissociation constants (K*d*) were as strong as L12-CTD•EF-G interaction (20), ranging between 0.1 and 0.4 mM (Supplementary Table S2). When the molar ratio of EF4 to L12-CTD reached 0.8 (Figure 6A, last panel and Figure 6C), most cross-peaks showed an apparent intensity decrease, indicating the formation of a large complex L12-CTD•EF4. In the 3D

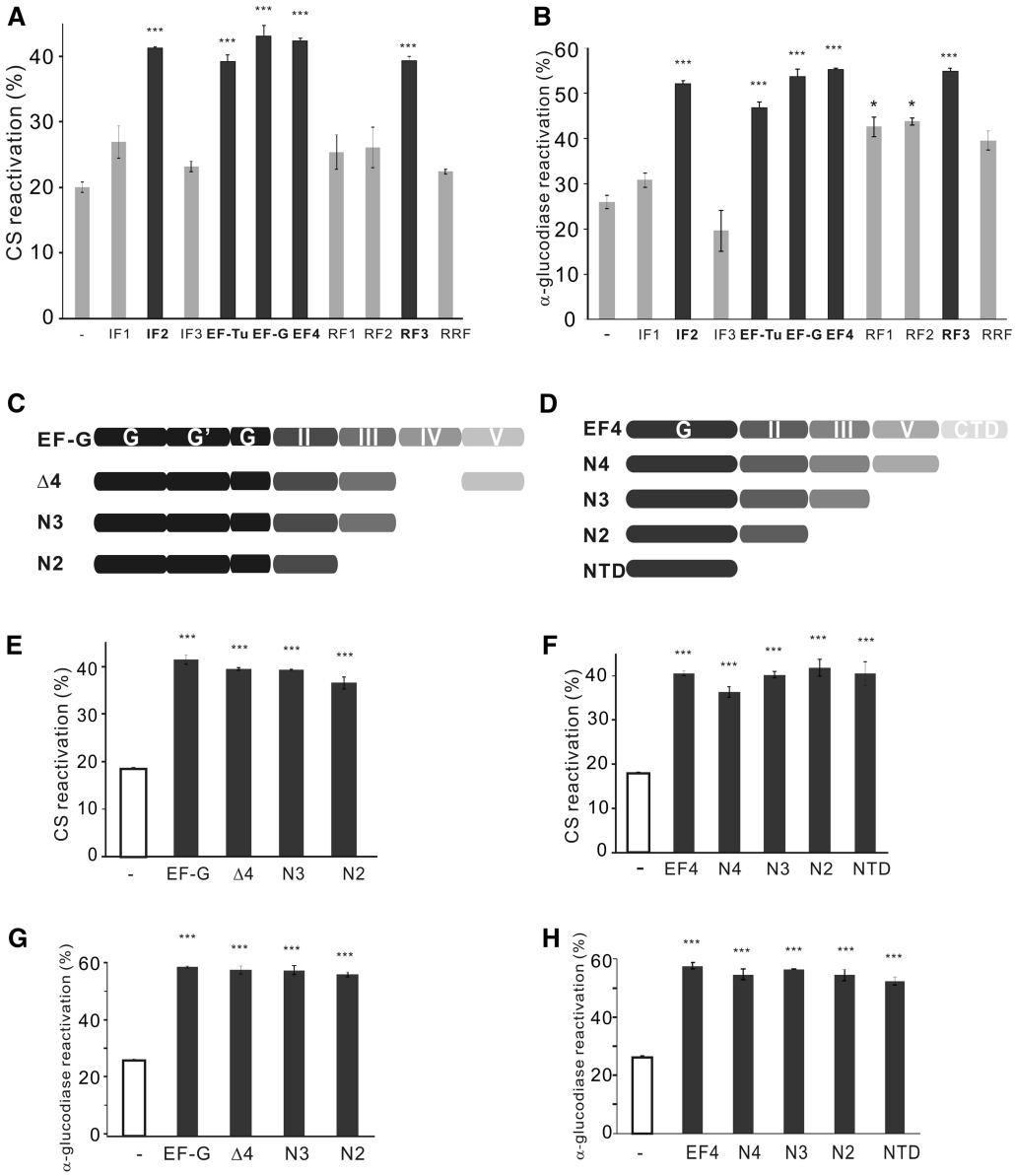

Figure 5. Common chaperone activity on the G-domains of trGTPase. (**A** and B) Chaperone activity of trGTPases. Denatured CS (**A**) or α-glucosidase (**B**) in the absence (−) and presence of translational factors was studied in a refolding assay. Denatured protein (0.1 μM) was incubated in the absence and presence of 5 μM translational factor. Similar to EF4, all trGTPases (black) showed chaperone activity, while all other translational factors (gray) exhibited much lower values, close to the negative control (−). (**C–H**) The G-domain of trGTPases is a chaperone activity center. To localize the enzymatic center, EF-G (**C**) or EF4 (**D**) was truncated as indicated. Full length and truncated proteins were studied in the CS (**E, F**) and α-glucosidase (**G, H**) refolding assays. Denatured protein (0.1 μM) was incubated in the absence (−) and presence of 5 μM of the factor constructs. Error bars represent the mean ± SEM of data from at least three separate experiments. *P*-values were calculated with unpaired *t*-test with Welch's correction by comparing to full length EF-G or EF4 samples, ($*P < 0.05$, $***P < 0.001$). See also Supplementary Figure S5 and Supplementary Table S1.

structure, the residues with large chemical shift changes are located on the lower right-hand side of L12-CTD (Figure 6D), which is very similar to the interaction region of L12-CTD with EF-G (20). These results support our hypothesis that EF4, like all other universal trGTPases, interacts with L12-CTD in a similar manner.

Finally, the influence of trGTPases on the L11–L12 interaction was analyzed in three NMR titration series. First, L11 protein was titrated into a solution of ^{15}N-L12-CTD, both proteins being from *E. coli*. At a physiological molar ratio of L11:L12-CTD = 1:4, some cross-peaks showed an intensity decrease (Figure 6E, green series). Corresponding residues showing a dramatic decrease were around Lys95 and cross-peak intensity decreased to ~80% of the initial intensity before L11 titration. When we added more L11 into L12-CTD, there was no further change, i.e. the interaction had been saturated. Second, EF-G (*E. coli*) was titrated into ^{15}N-L12-CTD, as a control. Both chemical shift changes and cross-peak intensity decrease were similar to those for EF4 (Figure 6E, pink series). We did not use EF4 (*T. thermophilus*) since the proteins precipitated at high

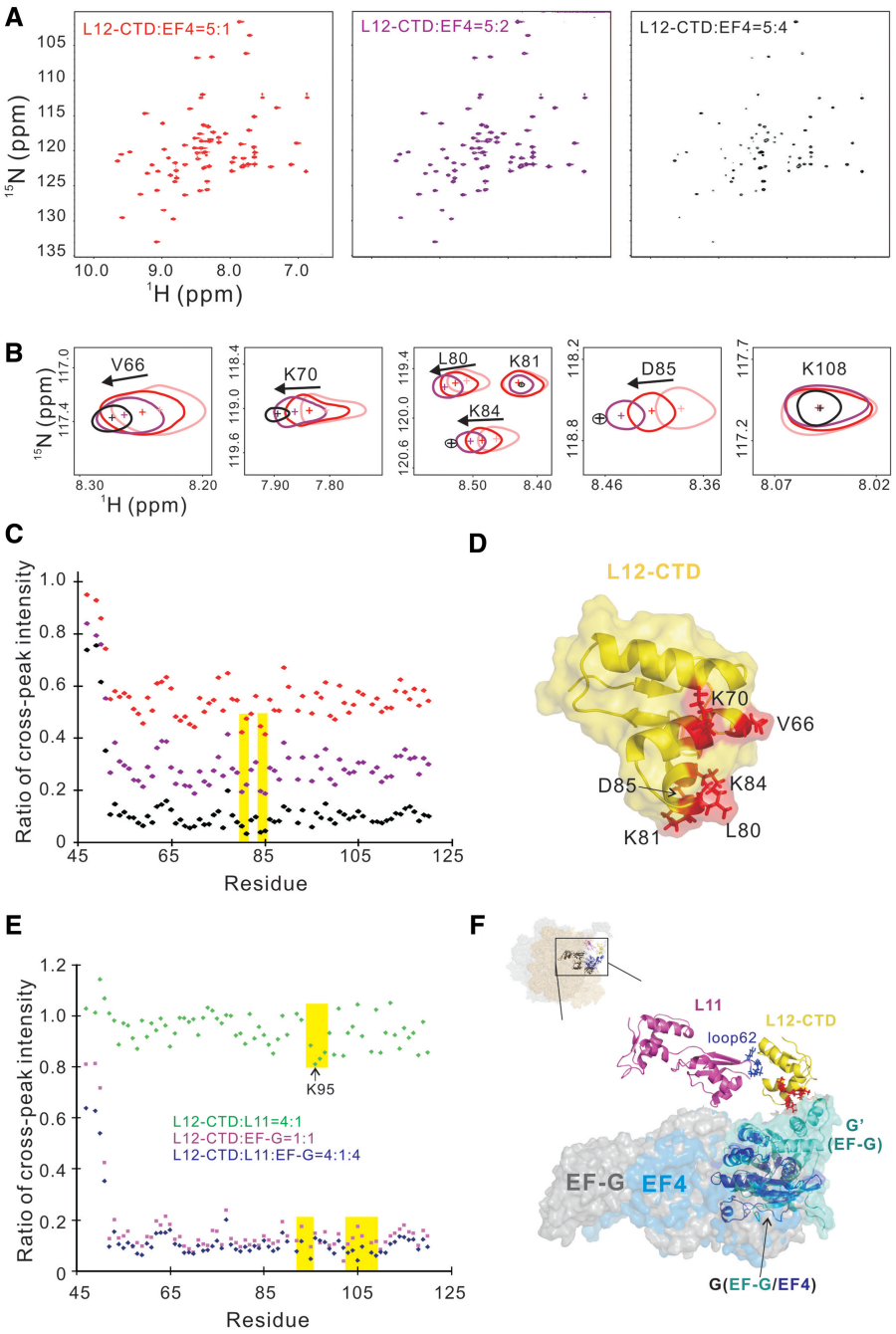

Figure 6. TrGTPase facilitates L11–L12 interaction *in vitro*. (**A–C**) NMR analysis of L12-CTD•EF4 interaction. (**A**) ^{1}H-^{15}N HSQC spectra of the ^{15}N-labeled L12-CTD (*E. coli*) titrated with EF4 (*T. thermophilus*) at different ratios. (**B**) A close-up view of the cross-peaks showing distinct changes in chemical shifts. The black arrow indicates the direction of the chemical shift. The K108 diagram is from a sample of the less affected cross-peak obtained by EF4 titration. (**C**) Cross-peak intensities of residues in L12-CTD plotted versus residue number. Varying molar ratios of EF4 to L12-CTD are colored as in A. Cross-peak intensities were evaluated as peak heights. Data were normalized using the intensities before EF4 titration. The highlighted regions (residues 78–86) exhibit comparably strong decrease in intensity. (**D**) Spatial locations of the residues on L12-CTD that are responsible for interacting with EF4. (**E**) L12-CTD was titrated by L11 or EF-G or both proteins. Scales of axes are the same as in C. Data were normalized using the intensity before titration. The highlighted regions exhibited comparably strong decreases in intensity. (**F**) EF4 from the cryo-EM structure of 70S•EF4•GDPNP in the PRE state (PDB 3DEG) (33) aligned with the EF-G in the crystal structure in (2WRL) (22). The G-domains of EF4 (blue) and EF-G (cyan) are represented as cartoons. The G′ domain of EF-G contacts L12-CTD from the lower right-hand side. Red residues in L12-CTD are the same as in D, namely those interacting EF4. It suggests the G-domain of EF4 might interact with the L12-CTD in a similar way as EF-G. See also Supplementary Figure S6 and Supplementary Table S2.

molar ratio to ^{15}N-L12-CTD. Third, EF-G was added to L12-CTD + L11 at a physiological molar ratio. Compared to the control (Figure 6E, pink series), most cross-peaks exhibited decreases in intensity to various extents (Figure 6E, dark blue series). Two regions of L12-CTD were strongly influenced due to the presence of both L11 and EF-G. Residues 92–95 and 103–109 decreased 40–50% and 50–70%, respectively.

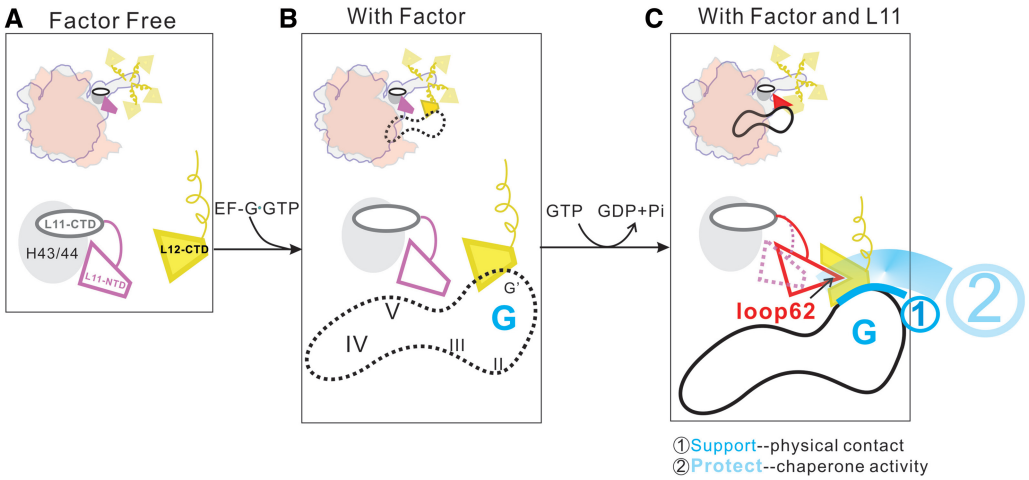

Figure 7. A 'Support-and-Protect' model of the L11–L12 interaction protected by the G-domain chaperone. (**A**) The ribosome is in the "Factor-Free" state that L12-CTD (yellow) protruding from the body of the ribosome has no interaction with L11-NTD (magenta). (**B**) Upon trGTPase loading, i.e. EF-G (dotted), L12-CTD initiates the interaction of the factor with the ribosome— "With Factor" state. (**C**) After EF-G fully docked and triggered *cis-trans* isomerization of PS22, L11-NTD (from magenta to red) inserts into L12-CTD, which has now an open conformation. Here, L12-CTD is in the state of "With Factor and L11". EF-G from the lower right-hand side supports and protects L12-CTD. For details, see the text and Supplementary Movie S1.

This intensity decrease indicates that there was a slow rotational correlation time, attributable to a secondary binding site. Hence, upon addition of EF-G, both the Lys95 and L106 regions were found to interact with L11, suggesting that the trGTPase facilitated the interaction between L11 and L12.

When we extracted the EF4 structure from PRE•EF4•GDPNP complex (PDB 3DEG) (33) and aligned it with EF-G on its POST•EF–G•FA complex, we found that EF4 had no opportunity to contact L12-CTD, since it has no G′-domain (Figure 6F). However, our NMR results demonstrate that the interaction between EF4 and L12-CTD is as strong as for EF-G and the contacting residues are almost the same. This observation suggests that trGTPases without G′-domain, such as EF4, should interact with L12-CTD in a very similar manner as trGTPases possessing a G′-domain. Based on the 3D structures, we conclude that it is the G-domain of these trGTPases that is responsible for this interaction. Collectively, our data suggest that the G-domain of all trGTPases harbors a chaperone activity which plays an important role in stabilizing the transiently exposed hydrophobic core of L12-CTD.

DISCUSSION

Here, we have demonstrated that L11-NTD interacts directly with L12-CTD through both a salt-bridge and hydrophobic stacking. This interaction is important for trGTPase docking onto the ribosome, the translation efficiency of the machinery and eventually the growth of the cell. Upon interacting with L11-NTD, L12-CTD transiently exposes the hydrophobic core, which may be protected and stabilized by the common chaperone activity of the G-domains of all trGTPases.

Our analysis of the direct interaction between L11 and L12 sheds light on cooperative dynamics between these two highly mobile domains at the tRNA and factor entrance of the ribosome. L12-CTD, by interacting with the G-domain of trGTPase, initiates the recruitment of translation factors. The attachment of L12-CTD is necessary for the function of the factor on the ribosome, such as GTPase activation and Pi release and factor recycling. On the other hand, L11-NTD is involved in regulating and fine-tuning the same set of activities of trGTPases; its regulatory ability is abolished when it is fixed by Thio or Micro. Thio prevents the interaction of L11-NTD with L12-CTD, while Micro blocks it. Our analysis of the direct interaction between L11-NTD and L12-CTD suggests that the highly flexible L11-NTD will be stabilized by L12-CTD upon factor binding, thus maintain: (i) the conformational stability of L12-CTD and (ii) the contact of L12-CTD with the G-domain of the trGTPase (Figure 6F).

We recently reported that a conserved structural switch in L11-NTD, namely proline switch 22 (PS22), composed of prolyl residues 21 and 22, is a determinant of the loop62 mobility. Upon *cis–trans* isomerization of PS22, loop62 undergoes a conformational transition between extended and retracted forms (34). Here we find that the extended loop62 connects L11-NTD with L12-CTD. Both the L11-D63•L12-K95 salt bridge and the hydrophobic surroundings contribute to the affinity. Upon loop62 insertion, L12-CTD adopts an open conformation exposing central hydrophobic residues, which could adversely affect the stability of the domain. Our results suggest that the chaperone activity of the G-domain of the uploaded trGTPase might stabilize the L12-CTD without restricting the flexibility of L12-CTD. Subsequently, L12-CTD in its optimal position and conformation is able to regulate the functions of trGTPase on the ribosome.

Our results indicate a reciprocal relationship between the ribosome and its factors. Importantly, the same

mechanism is observed in all phases of translation when a trGTPase is recruited, i.e. initiation, elongation, termination and recycling. This suggests that, in every step involving a trGTPase, the physical support and chaperone protection of L12-CTD by trGTPase is required. From the literature (1,3,4,7,8,12,15,20) and our data we can distinguish three states that L12-CTD can adopt during the recruitment of a trGTPase. The first state is the factor-free state, where L12-CTD protruding from the body of the ribosome is highly dynamic in solution; L11-NTD has no contact with L12-CTD (Figure 7A). Second, L12-CTD initiates factor recruitment by interacting with the G-domain of a trGTPase; the factor is in the process of being dock into the ribosome. Here, L12-CTD interacts with the trGTPase, but is not yet connected with L11 (Figure 7B). Third, after the factor has fully docked on the ribosome and catalyzed the *cis–trans* isomerization of PS22, loop62 of L11-NTD will be inserted into L12-CTD, forcing the exposure of its hydrophobic core. In this step, the G-domain of the factor facilitates the interaction with L12-CTD. This interaction has two functional aspects: (i) it provides physical support of the G-domain for L12-CTD and maintains the L12-CTD•L11-NTD interactions and (ii) the chaperone activity of the G-domain protects the open conformer of L12-CTD: the G-domain surrounds L12-CTD to prevent it from unfolding. Thus, a trGTPase, instead of being passively regulated by the ribosome, contributes to the dynamics of the L11-NTD•L12-CTD connection (Figure 7 and Supplementary Movie S1). Our data suggest that this universal mechanism for the docking of a trGTPase is important for the high efficiency of protein biosynthesis.

SUPPLEMENTARY DATA

Supplementary Data are available at NAR Online: Supplementary Tables 1 and 2, Supplementary Figures 1–6, Supplementary Methods, Supplementary Movie 1 and Supplementary references [38–40].

ACKNOWLEDGEMENTS

We thank Prof. Joachim Frank and Dr Jesper Pallesen (Columbia University), Profs Congzhao Zhou (USTC) and Wei Feng (Institute of Biophysics, CAS) for help and discussions, Dr. Joy Fleming for English editing, Dejiu Zhang, Ping Zhao, Liujuan Cui and Xiang Wang for technical support. We thank the Supercomputing Center of Chinese Academy of Sciences (SCCAS) for providing us the computational recourses.

FUNDING

Major State Basic Research of China 973 [2012CB911001 to Y.Q. and 2011CB910503 to W.G.]; National Natural Science Foundation of China [31170756, 31270847 to Y.Q. and 31021062 to W.G.]; Novo Nordisk—Chinese Academy of Sciences Research Foundation [to Y.Q.] Funding for open access charge: Major State Basic Research of China 973 [2011CB910503 to W.G.].

Conflict of interest statement. None declared.

REFERENCES

1. Diaconu,M., Kothe,U., Schlunzen,F., Fischer,N., Harms,J.M., Tonevitsky,A.G., Stark,H., Rodnina,M.V. and Wahl,M.C. (2005) Structural basis for the function of the ribosomal L7/12 stalk in factor binding and GTPase activation. *Cell*, **121**, 991–1004.
2. Traut,R.R., Dey,D., Bochkariov,D.E., Oleinikov,A.V., Jokhadze,G.G., Hamman,B. and Jameson,D. (1995) Location and domain structure of Escherichia coli ribosomal protein L7/L12: site specific cysteine cross-linking and attachment of fluorescent probes. *Biochem. Cell Biol.*, **73**, 949–958.
3. Agrawal,R.K., Linde,J., Sengupta,J., Nierhaus,K.H. and Frank,J. (2001) Localization of L11 protein on the ribosome and elucidation of its involvement in EF-G-dependent translocation. *J. Mol. Biol.*, **311**, 777–787.
4. Christodoulou,J., Larsson,G., Fucini,P., Connell,S.R., Pertinhez,T.A., Hanson,C.L., Redfield,C., Nierhaus,K.H., Robinson,C.V., Schleucher,J. *et al.* (2004) Heteronuclear NMR investigations of dynamic regions of intact Escherichia coli ribosomes. *Proc. Natl Acad. Sci. USA*, **101**, 10949–10954.
5. Kavran,J.M. and Steitz,T.A. (2007) Structure of the base of the L7/L12 stalk of the Haloarcula marismortui large ribosomal subunit: analysis of L11 movements. *J. Mol. Biol.*, **371**, 1047–1059.
6. Agrawal,R.K., Heagle,A.B., Penczek,P., Grassucci,R.A. and Frank,J. (1999) EF-G-dependent GTP hydrolysis induces translocation accompanied by large conformational changes in the 70S ribosome. *Nat. Struct. Biol.*, **6**, 643–647.
7. Datta,P.P., Sharma,M.R., Qi,L., Frank,J. and Agrawal,R.K. (2005) Interaction of the G′ domain of elongation factor G and the C-terminal domain of ribosomal protein L7/L12 during translocation as revealed by cryo-EM. *Mol. Cell*, **20**, 723–731.
8. Ratje,A.H., Loerke,J., Mikolajka,A., Brunner,M., Hildebrand,P.W., Starosta,A.L., Donhofer,A., Connell,S.R., Fucini,P., Mielke,T. *et al.* (2010) Head swivel on the ribosome facilitates translocation by means of intra-subunit tRNA hybrid sites. *Nature*, **468**, 713–716.
9. Donner,D., Villems,R., Liljas,A. and Kurland,C.G. (1978) Guanosinetriphosphatase activity dependent on elongation factor Tu and ribosomal protein L7/L12. *Proc. Natl Acad. Sci. USA*, **75**, 3192–3195.
10. Mohr,D., Wintermeyer,W. and Rodnina,M.V. (2002) GTPase activation of elongation factors Tu and G on the ribosome. *Biochemistry*, **41**, 12520–12528.
11. Kothe,U., Wieden,H.J., Mohr,D. and Rodnina,M.V. (2004) Interaction of helix D of elongation factor Tu with helices 4 and 5 of protein L7/12 on the ribosome. *J. Mol. Biol.*, **336**, 1011–1021.
12. Savelsbergh,A., Mohr,D., Kothe,U., Wintermeyer,W. and Rodnina,M.V. (2005) Control of phosphate release from elongation factor G by ribosomal protein L7/12. *EMBO J.*, **24**, 4316–4323.
13. Lentzen,G., Klinck,R., Matassova,N., Aboul-ela,F. and Murchie,A.I. (2003) Structural basis for contrasting activities of ribosome binding thiazole antibiotics. *Chem. Biol.*, **10**, 769–778.
14. Jonker,H.R.A., Ilin,S., Grimm,S.K., Wohnert,J. and Schwalbe,H. (2007) L11 domain rearrangement upon binding to RNA and thiostrepton studied by NMR spectroscopy. *Nucleic Acids Res.*, **35**, 441–454.
15. Harms,J.M., Wilson,D.N., Schluenzen,F., Connell,S.R., Stachelhaus,T., Zaborowska,Z., Spahn,C.M. and Fucini,P. (2008) Translational regulation via L11: molecular switches on the ribosome turned on and off by thiostrepton and micrococcin. *Mol. Cell*, **30**, 26–38.
16. Cundliffe,E. and Thompson,J. (1981) Concerning the mode of action of micrococcin upon bacterial protein synthesis. *Eur. J. Biochem.*, **118**, 47–52.
17. Pestka,S. (1970) Thiostrepton: a ribosomal inhibitor of translocation. *Biochem. Biophys. Res. Commun.*, **40**, 667–674.
18. Mikolajka,A., Liu,H., Chen,Y., Starosta,A.L., Marquez,V., Ivanova,M., Cooperman,B.S. and Wilson,D.N. (2011) Differential effects of thiopeptide and orthosomycin antibiotics on translational GTPases. *Chem. Biol.*, **18**, 589–600.

19. Mulder,F.A., Bouakaz,L., Lundell,A., Venkataramana,M., Liljas,A., Akke,M. and Sanyal,S. (2004) Conformation and dynamics of ribosomal stalk protein L12 in solution and on the ribosome. *Biochemistry*, **43**, 5930–5936.
20. Helgstrand,M., Mandava,C.S., Mulder,F.A., Liljas,A., Sanyal,S. and Akke,M. (2007) The ribosomal stalk binds to translation factors IF2, EF-Tu, EF-G and RF3 via a conserved region of the L12 C-terminal domain. *J. Mol. Biol.*, **365**, 468–479.
21. Li,W., Sengupta,J., Rath,B.K. and Frank,J. (2006) Functional conformations of the L11-ribosomal RNA complex revealed by correlative analysis of cryo-EM and molecular dynamics simulations. *RNA*, **12**, 1240–1253.
22. Gao,Y.G., Selmer,M., Dunham,C.M., Weixlbaumer,A., Kelley,A.C. and Ramakrishnan,V. (2009) The structure of the ribosome with elongation factor G trapped in the posttranslocational state. *Science*, **326**, 694–699.
23. Qin,Y., Polacek,N., Vesper,O., Staub,E., Einfeldt,E., Wilson,D.N. and Nierhaus,K.H. (2006) The highly conserved LepA is a ribosomal elongation factor that back-translocates the ribosome. *Cell*, **127**, 721–733.
24. Szaflarski,W., Vesper,O., Teraoka,Y., Plitta,B., Wilson,D.N. and Nierhaus,K.H. (2008) New features of the ribosome and ribosomal inhibitors: non-enzymatic recycling, misreading and back-translocation. *J. Mol. Biol.*, **380**, 193–205.
25. Caldas,T., Laalami,S. and Richarme,G. (2000) Chaperone properties of bacterial elongation factor EF-G and initiation factor IF2. *J. Biol. Chem.*, **275**, 855–860.
26. Jakob,U., Gaestel,M., Engel,K. and Buchner,J. (1993) Small heat shock proteins are molecular chaperones. *J. Biol. Chem.*, **268**, 1517–1520.
27. Humphrey,W., Dalke,A. and Schulten,K. (1996) VMD: visual molecular dynamics. *J. Mol. Graph.*, **14**, 33–38, 27–38.
28. Phillips,J.C., Braun,R., Wang,W., Gumbart,J., Tajkhorshid,E., Villa,E., Chipot,C., Skeel,R.D., Kale,L. and Schulten,K. (2005) Scalable molecular dynamics with NAMD. *J. Comput. Chem.*, **26**, 1781–1802.
29. Leijonmarck,M. and Liljas,A. (1987) Structure of the C-terminal domain of the ribosomal protein L7/L12 from Escherichia coli at 1.7 A. *J. Mol. Biol.*, **195**, 555–579.
30. Foloppe,N. and MacKerell,A.D. (2000) All-atom empirical force field for nucleic acids: I. Parameter optimization based on small molecule and condensed phase macromolecular target data. *J. Comput. Chem.*, **21**, 86–104.
31. Walter,J.D., Hunter,M., Cobb,M., Traeger,G. and Spiegel,P.C. (2012) Thiostrepton inhibits stable 70S ribosome binding and ribosome-dependent GTPase activation of elongation factor G and elongation factor 4. *Nucleic Acids Res.*, **40**, 360–370.
32. Markus,M.A., Triantafillidou,D., Choli-Papadopoulou,T. and Torchia,D.A. (2001) 1 H, 15 N, and 13 C assignments and secondary structure identification for full-length ribosomal protein L11 from Thermus thermophilus. *J. Biomol. NMR*, **20**, 293–294.
33. Connell,S.R., Topf,M., Qin,Y., Wilson,D.N., Mielke,T., Nierhaus,K.H. and Sphan,C.M. (2008) A new tRNA intermediate revealed on the ribosome during EF4-mediated back-translocation. *Nat. Struct. Mol. Biol.*, **15**, 910–915.
34. Wang,L., Yang,F., Zhang,D., Chen,Z., Xu,R.M., Nierhaus,K.H., Gong,W. and Qin,Y. (2012) A conserved proline switch on the ribosome facilitates the recruitment and binding of trGTPases. *Nat. Struct. Mol. Biol.*, **19**, 403–410.
35. Hartl,F.U., Bracher,A. and Hayer-Hartl,M. (2011) Molecular chaperones in protein folding and proteostasis. *Nature*, **475**, 324–332.
36. Caldas,T.D., El Yaagoubi,A. and Richarme,G. (1998) Chaperone properties of bacterial elongation factor EF-Tu. *J. Biol. Chem.*, **273**, 11478–11482.
37. Evans,R.N., Blaha,G., Bailey,S. and Steitz,T.A. (2008) The structure of LepA, the ribosomal back translocase. *Proc. Natl Acad. Sci. USA*, **105**, 4673–4678.
38. Bocharov,E.V., Gudkov,A.T. and Arseniev,A.S. (1996) Topology of the secondary structure elements of ribosomal protein L7/L12 from E. coli in solution. *FEBS Lett.*, **379**, 291–294.
39. Johnson,B.A. (2004) Using NMRView to visualize and analyze the NMR spectra of macromolecules. *Methods Mol. Biol.*, **278**, 313–352.
40. Krebs,W.G. (2000) Gerstein M. SURVEY AND SUMMARY The morph server: a standardized system for analyzing and visualizing macromolecular motions in a database framework. *Nucleic Acids Res.*, **28**, 1665–1675.